A Unified Model for Color Prediction of Halftoned Prints

Patrick Emmel▲ and Roger David Hersch

Ecole Polytechnique Fédérale de Lausanne (EPFL), Département d'Informatique, Laboratoire de Systèmes Périphériques, Lausanne, Switzerland

This study introduces a new model and a new mathematical formulation describing the light scattering and ink spreading phenomena in printing. The new model generalizes the classical Kubelka–Munk theory, and unifies it with the Neugebauer model within a single mathematical framework based on matrices. Results like the Saunderson correction, the Clapper–Yule equation, the Murray–Davis relation and the Williams–Clapper equation are shown to be particular cases of the new model. Using this new theoretical tool, the reflection spectra of 100 samples printed on high quality paper by two different ink-jet printers were computed with an average prediction error of about $\Delta E = 2.1$ in CIELAB.

Journal of Imaging Science and Technology 44: 351–359 (2000)

Introduction

Several physical phenomena influence colors reproduced by ink-jet printers. This makes accurate color prediction very difficult. The dot gain effect is generally considered to have the largest impact on color deviations. Dot gain is caused by light scattering or by ink spreading or both together.

Although intensive investigations on optical dot gain (Yule–Nielsen effect) have been made recently,[1,2,3] the resulting prediction models are still very complex. In this article we propose a global approach that incorporates all physical-contributing phenomena into a single model using a mathematical framework based on matrices. We will show that classical results (for example the Clapper–Yule relation) correspond to particular cases of our model.

According to our experience in ink-jet printing, light scattering is not the only process that induces color deviations. When ink drops are printed over each other or just overlap partially, an ink spreading process takes place that also modifies the printed color in a significant way. A model is proposed and applied to predict accurately the spectra of real samples produced with two inks on two different ink-jet printers.

Matrix Form of the Kubelka–Munk Model

Let us consider a reflector made of a reflecting substrate of reflectance R_g in optical contact with a light absorbing and light scattering medium of thickness X (see Fig. 1). Kubelka and Munk[4] proposed a reflection model based on two light fluxes: $i(x)$ oriented downwards and $j(x)$ oriented upwards.

The variation of $i(x)$ and $j(x)$ when they cross an infinitesimal layer of thickness dx is given by the system of linear differential equations:

$$\begin{cases} \dfrac{di(x)}{dx} = (K+S)i(x) - Sj(x) \\ \dfrac{dj(x)}{dx} = -(K+S)j(x) + Si(x) \end{cases} \quad (1)$$

where K is the light absorption coefficient and S the light scattering coefficient of the medium. Note that in a transparent medium S equals 0 and the differential equation, Eq. 1, leads to Beer's law.

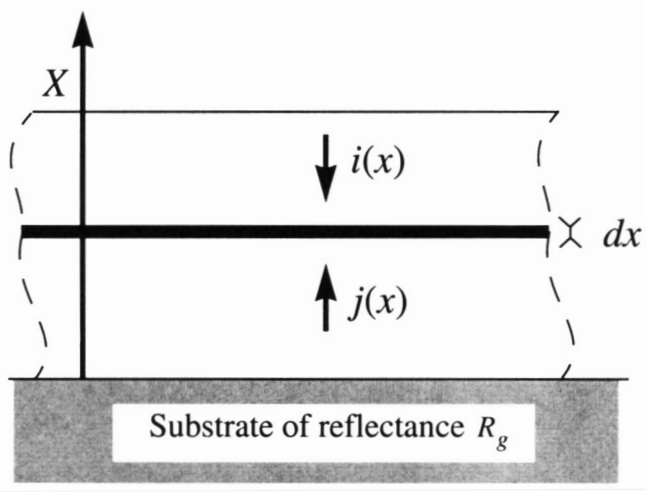

Figure 1. An ink-absorbing medium of thickness X is in optical contact with a substrate of reflectance R_g. This medium is divided into parallel layers of infinitesimal thickness dx. Two fluxes are considered: $i(x)$ oriented downwards and $j(x)$ oriented upwards.

Original manuscript received December 15, 1999

▲ IS&T Member

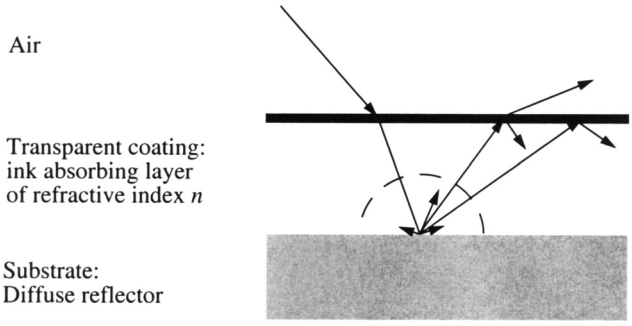

Figure 2. Multiple internal reflections caused by the interface between the air and the transparent coating.

The system in Eq. 1 can be written in matrix form:

$$\begin{bmatrix} \dfrac{di(x)}{dx} \\ \dfrac{dj(x)}{dx} \end{bmatrix} = \begin{bmatrix} K+S & -S \\ S & -(K+S) \end{bmatrix} \cdot \begin{bmatrix} i(x) \\ j(x) \end{bmatrix}. \tag{2}$$

This kind of matrix differential equation has a well known solution which is given by the exponential of the matrix.[5] By integrating the equation between $x = 0$ and $x = X$ we get:

$$\begin{bmatrix} i(X) \\ j(X) \end{bmatrix} = \exp\left(\begin{bmatrix} K+S & -S \\ S & -(K+S) \end{bmatrix} (X-0) \right) \cdot \begin{bmatrix} i(0) \\ j(0) \end{bmatrix}, \tag{3}$$

where $i(0)$ and $j(0)$ are the intensities of the fluxes i and j at $x = 0$. Note that the exponential of a matrix M is defined by the following power series:

$$\exp(M) = \sum_{i=0}^{\infty} \frac{(M)^i}{i!}. \tag{4}$$

The ratio $\rho = j(X)/i(X)$ is called the body (or true) reflectance[6] of the analyzed sample. It corresponds to an internal reflection coefficient that does not take multiple internal reflections into account (see next section). From Eq. 3 and the boundary condition $j(0) = R_g \cdot i(0)$, we can derive by algebraic manipulations[7,8] all the well-known results of the Kubelka–Munk theory which are listed in the literature.[9]

Model of High Quality Paper and Saunderson Correction

In the present study, we consider high quality ink-jet paper consisting of an ink-absorbing layer in optical contact with the substrate that is a diffuse white reflector of reflectance R_g. This reflector is supposed to be Lambertian[10] and is never in contact with the inks. Because the transparent coating has a refractive index n different from that of air, multiple internal reflections occur[11] as shown in Fig. 2. This phenomenon significantly increases the optical density of the ink-containing layer. Traditionally, this is taken into account by applying the Saunderson correction[12] to the computed spectrum. In this section, we write the Saunderson correction in matrix form, to be applied to Eq. 3.

Let us denote by i the incident flux on the external surface of the paper and by j the flux emerging from the paper. Let r_s be the fraction of diffuse light reflected by the air-coating interface (external surface of the paper), and let r_i be the fraction of diffuse light reflected by the air-coating interface (internal surface of paper). The values of r_s and r_i depend only on the refractive index of the transparent coating. Judd[13] has computed their numerical values for a large number of refractive indices.

The balance of the fluxes at the air-coating interface, as shown in Fig. 3, leads to the following system of equations for $i(X)$, the incident flux below the air-coating interface and for j, the emerging flux above the air-coating interface:

$$\begin{aligned} i(X) &= (1-r_s)i + r_i j(X) \\ j &= r_s i + (1-r_i) j(X) \end{aligned} \tag{5}$$

Assuming that the refractive index of the coating is constant over the whole visible range of wavelengths, r_s and r_i are also constant. Hence, Eq. 5 can be written in the following matrix form:

$$\begin{bmatrix} i \\ j \end{bmatrix} = \begin{bmatrix} \dfrac{1}{1-r_s} & \dfrac{-r_i}{1-r_s} \\ \dfrac{r_s}{1-r_s} & \left(1-r_i-\dfrac{r_s r_i}{1-r_s}\right) \end{bmatrix} \cdot \begin{bmatrix} i(X) \\ j(X) \end{bmatrix}. \tag{6}$$

The Saunderson correction is obtained by combining Eq. 6 and Eq. 3:

$$\begin{aligned} \begin{bmatrix} i \\ j \end{bmatrix} &= \begin{bmatrix} \dfrac{1}{1-r_s} & \dfrac{-r_i}{1-r_s} \\ \dfrac{r_s}{1-r_s} & \left(1-r_i-\dfrac{r_s r_i}{1-r_s}\right) \end{bmatrix} \\ &\quad \cdot \exp\left(\begin{bmatrix} K+S & -S \\ S & -(K+S) \end{bmatrix} X \right) \cdot \begin{bmatrix} i(0) \\ j(0) \end{bmatrix} \\ &= \begin{bmatrix} t & u \\ v & w \end{bmatrix} \cdot \begin{bmatrix} i(0) \\ j(0) \end{bmatrix}. \end{aligned} \tag{7}$$

We denote the elements of the product matrix by t, u, v and w. These coefficients and the boundary condition $j(0) = R_g \cdot i(0)$ allow the calculation of the reflection coefficient R:

$$R = \frac{j}{i} = \frac{t + R_g \cdot u}{v + R_g \cdot w}. \tag{8}$$

This equation allows us to compute the reflection spectrum of a light-absorbing and light-scattering medium in optical contact with a substrate of known reflectance R_g. If we develop the product in Eq. 8 algebraically, we obtain the famous Saunderson corrected reflection formula.[14]

When using the 45°/0° measuring geometry instead of diffuse light as assumed here, the matrix in Eq. 6 must be modified as shown in Ref. 15. Note that this modified matrix leads, after developing Eq. 8, to the Williams–Clapper equation.[16]

The interesting aspect of our present approach is the matrix formulation of Eq. 7 that gives a better overview of the modeled system. Instead of using several functions incorporated within each other, the analyzed sample is simply modeled by the product of two matrices.

New Mathematical Framework for Light Scattering in the Substrate

The Kubelka–Munk model presented in the previous sections assumes that the ink-absorbing layer is uniform, i.e. that it contains the same amount of dye everywhere. In halftone prints, this is no longer true because ink was not applied uniformly over the whole surface. Due to light scattering in the substrate (paper), a photon can penetrate the paper through an inked region and leave the paper through a non-inked region, or vice versa.

In a first step, we generalize the previous model by taking only two types of regions into account: inked and non-inked. Furthermore, since the ink-absorbing layer is very thin (about 10 μm), we assume that the exchange of photons between surface elements only takes place in the substrate. We also assume that each surface element behaves according to the Kubelka–Munk model described previously.

Let us now consider such a surface having only two different inking levels. As for the Kubelka–Munk model, we define for each inking level two light fluxes: i_k oriented downwards and j_k oriented upwards. The index k takes the value 0 for the non-inked region and 1 for the inked region (see Fig. 4).

The matrix in Eq. 2 can be extended in order to take several inking levels into account. Let us denote M_{KS} this extended block matrix. For two inking levels, the equation can be written as follows:

$$\frac{d}{dx}\begin{bmatrix} i_0(x) \\ j_0(x) \\ i_1(x) \\ j_1(x) \end{bmatrix} = M_{KS} \cdot \begin{bmatrix} i_0(x) \\ j_0(x) \\ i_1(x) \\ j_1(x) \end{bmatrix} \tag{9}$$

$$= \begin{bmatrix} K_0 + S_0 & -S_0 & 0 & 0 \\ S_0 & -(K_0 + S_0) & 0 & 0 \\ 0 & 0 & K_1 + S_1 & -S_1 \\ 0 & 0 & S_1 & -(K_1 + S_1) \end{bmatrix} \cdot \begin{bmatrix} i_0(x) \\ j_0(x) \\ i_1(x) \\ j_1(x) \end{bmatrix},$$

where K_0, S_0, K_1 and S_1 are respectively the absorption and scattering coefficients of the non-inked medium and the inked medium. By integrating Eq. 9 between $x = 0$ and $x = X$ we get:

$$\begin{bmatrix} i_0(X) \\ j_0(X) \\ i_1(X) \\ j_1(X) \end{bmatrix} = \exp\left(M_{KS} \cdot X\right) \cdot \begin{bmatrix} i_0(0) \\ j_0(0) \\ i_1(0) \\ j_1(0) \end{bmatrix}. \tag{10}$$

The definition of the matrix exponential is given in Eq. 4.

In order to take into consideration the multiple internal reflections, the Saunderson correction must also be applied here. Note that in our case the ink is inside the medium and not on top of it. Hence the interface between the air and the ink-absorbing medium is the same in non-inked regions and in inked regions. Therefore, from Eq. 6 we can directly derive the resulting Saunderson correction matrix M_{SC}:

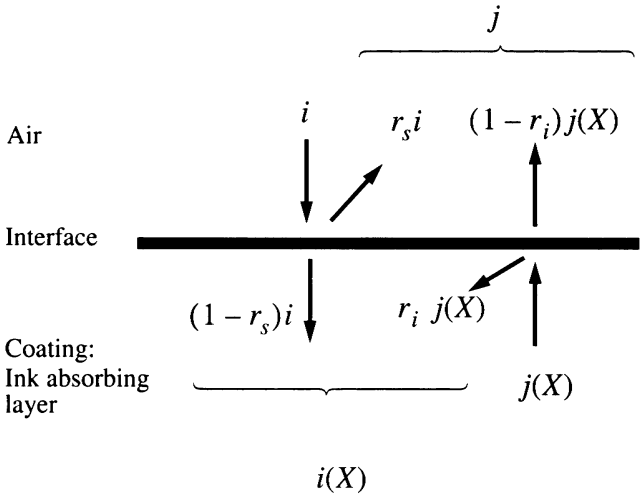

Figure 3. External and internal reflections of the upward and downward fluxes on the air-coating interface.

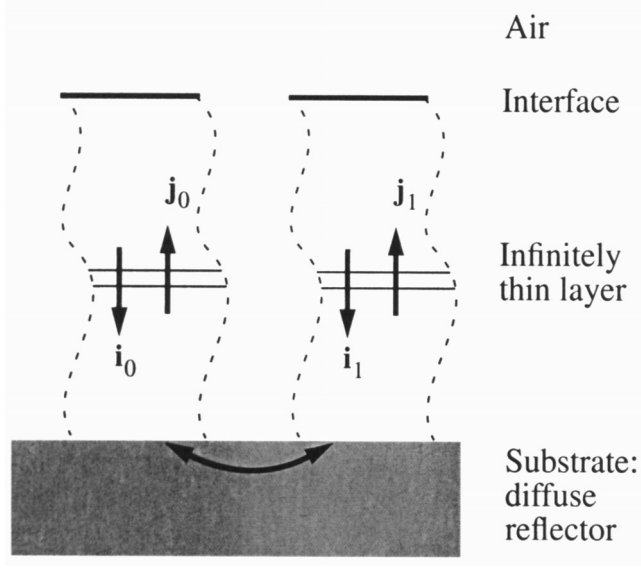

Figure 4. Schematic model of the printed surface. On top of the substrate, each surface-element is considered to be a uniform layer that behaves according to the Kubelka–Munk model. The exchange of photons between different regions takes place in the substrate.

$$\begin{bmatrix} i_0 \\ j_0 \\ i_1 \\ j_1 \end{bmatrix} = M_{SC} \cdot \begin{bmatrix} i_0(X) \\ j_0(X) \\ i_1(X) \\ j_1(X) \end{bmatrix} \tag{11}$$

$$= \begin{bmatrix} \frac{1}{1-r_s} & \frac{-r_i}{1-r_s} & 0 & 0 \\ \frac{r_s}{1-r_s} & \left(1 - r_i - \frac{r_s r_i}{1-r_s}\right) & 0 & 0 \\ 0 & 0 & \frac{1}{1-r_s} & \frac{-r_i}{1-r_s} \\ 0 & 0 & \frac{r_s}{1-r_s} & \left(1 - r_i - \frac{r_s r_i}{1-r_s}\right) \end{bmatrix} \cdot \begin{bmatrix} i_0(X) \\ j_0(X) \\ i_1(X) \\ j_1(X) \end{bmatrix}.$$

The key to our model lies in the way light scattering is expressed mathematically. We assume that the exchange of photons only takes place in the substrate, and therefore, light scattering only affects the boundary conditions at $x = 0$. This implies that the upward oriented fluxes $j_0(0)$ and $j_1(0)$ depend on downward oriented fluxes $i_0(0)$, $i_1(0)$ and the reflection coefficient R_g of the substrate. As shown in Eq. 12, this can be written in a general way under matrix form.

$$\begin{bmatrix} j_0(0) \\ j_1(0) \end{bmatrix} = R_g \cdot \begin{bmatrix} \delta_{0,0} & \delta_{0,1} \\ \delta_{1,0} & \delta_{1,1} \end{bmatrix} \cdot \begin{bmatrix} i_0(0) \\ i_1(0) \end{bmatrix}, \tag{12}$$

where the coefficient $\delta_{u,v}$ represents the overall probability of a photon entering through a surface element having the inking level v to emerge from a surface element having the inking level u. Note that the probability is taken throughout the full sample area. Arney[1,17] introduced this probabilistic approach. Because we deal with probabilities, the sum of the coefficient $\delta_{u,v}$ belonging to the same line of the matrix in Eq. 12 must equal 1. The computation of the scattering probabilities $\delta_{u,v}$ will be addressed in the next section.

Now we can put all elements together and write the matrix equation of our new prediction model. By combining Eqs. 10, 11 and 12 we obtain Eq. 13.

The first matrix of Eq. 13 represents the Saunderson correction, the second matrix corresponds to the Kubelka–Munk modeling of the ink absorbing layer and the third matrix models the light scattering in the substrate.

$$\begin{bmatrix} i_0 \\ j_0 \\ i_1 \\ j_1 \end{bmatrix} = M_{SC} \cdot \exp\left(M_{KS} \cdot X\right) \cdot \begin{bmatrix} 1 & 0 & 0 & 0 \\ 0 & \delta_{0,0} & 0 & \delta_{0,1} \\ 0 & 0 & 1 & 0 \\ 0 & \delta_{1,0} & 0 & \delta_{1,1} \end{bmatrix} \cdot \begin{bmatrix} i_0(0) \\ R_g i_0(0) \\ i_1(0) \\ R_g i_1(0) \end{bmatrix} \tag{13}$$

Computing the emerging fluxes j_0 and j_1 as functions of the incident fluxes i_0 and i_1 requires rearranging the lines and columns of the matrices. In order to keep the block structure of the matrices, we introduce a change of basis matrix as shown in Eq. 14. Note that this particular change of basis matrix is its own inverse. Furthermore, the last vector of Eq. 13 is written in Eq. 14 as the product of a 4×2 matrix by a two-dimensional vector.

After computing the matrix products in Eq. 14, we get a 4×2 matrix which can be split into two 2×2 matrices. The first matrix relates the vector $[i_0,i_1]$ to $[i_0(0),i_1(0)]$; and the second matrix relates $[j_0,j_1]$ to $[i_0(0),i_1(0)]$. By multiplying the second matrix by the inverse of the first matrix, we derive a relation that expresses the emerging fluxes j_0 and j_1 as linear functions of the incident fluxes i_0 and i_1.

Because the incident light has the same intensity on inked and non-inked regions, we have $i_0 = i_1 = i$. Let a_1 be the fraction of area occupied by inked regions, and $a_0 = 1 - a_1$ be the fraction of area occupied by non-inked regions. As in the Neugebauer model,[18] the reflection coefficient R of the whole surface is given by the weighted sum of the spectra of the emerging light divided by the spectra of the incident light; where the weights are the fractions of area occupied by the various ink combinations. Hence the final result is given by:

$$R = \frac{\begin{bmatrix} a_0 & a_1 \end{bmatrix} \cdot \begin{bmatrix} j_0 \\ j_1 \end{bmatrix}}{\begin{bmatrix} a_0 & a_1 \end{bmatrix} \cdot \begin{bmatrix} i_0 \\ i_1 \end{bmatrix}} = \frac{(1-a_1)j_0 + a_1 j_1}{i}. \tag{15}$$

Let us consider the particular case in which the average lateral light scattering distance is great compared to the size of the halftoning element. This is the assumption of complete scattering. In this case, for any inking level v, the probability $\delta_{u,v}$ equals the fraction of area a_u occupied by the inking level u:

$$\delta_{0,0} = \delta_{1,0} = a_0 = 1 - a_1 \text{ and } \delta_{0,1} = \delta_{1,1} = a_1 \tag{16}$$

By introducing Eq. 16 into Eq. 14 and assuming that $S_0 = 0$, $S_1 = 0$. $K_0 = 0$, we obtain from Eq. 15 the well-known Clapper–Yule[19] relation:

$$R = r_s + \frac{R_g(1-r_s)(1-r_i)(1-a_1+a_1T)^2}{1-R_g r_i(1-a_1+a_1T^2)} \tag{17}$$

where $T = \exp[-K_1X]$. Note that this calculation was done with the help of a mathematics software package.

In another particular case, lateral light scattering can be neglected. Hence, the probability of a photon being scattered in a region with a different inking level equals 0. This implies that $\delta_{u,u} = 1$ and $\delta_{u,v} = 0$ for $u \neq v$. In other words, the second last matrix of Eq. 14 is an identity matrix. In this case, assuming $S_0 = 0$, $S_1 = 0$, $K_0 = 0$, $r_i = 0$, $r_s = 0$ leads to the Murray–Davis relation:[20]

$$R = R_g\left[(1-a_1) + a_1T^2\right] \tag{18}$$

where $T = \exp[-K_1X]$.

Simplified Light Scattering Model

There are several methods that allow the computation of the scattering probabilities $\delta_{u,v}$. Most of these methods use a point spread function (PSF) which is generally assumed or measured empirically. The convolution between this function and the halftone pattern leads to the surface reflectance[21] from which the scattering probabilities are deduced. Further advanced models calculate the PSF based on a physical light scattering model.[22] Because these methods imply the use of operations such

$$\begin{bmatrix} i_0 \\ i_1 \\ j_0 \\ j_1 \end{bmatrix} = \begin{bmatrix} 1 & 0 & 0 & 0 \\ 0 & 0 & 1 & 0 \\ 0 & 1 & 0 & 0 \\ 0 & 0 & 0 & 1 \end{bmatrix} \cdot M_{SC} \cdot \exp\left(M_{KS} \cdot X\right) \cdot \begin{bmatrix} 1 & 0 & 0 & 0 \\ 0 & 0 & 1 & 0 \\ 0 & 1 & 0 & 0 \\ 0 & 0 & 0 & 1 \end{bmatrix}^{-1} \cdot \begin{bmatrix} 1 & 0 & 0 & 0 \\ 0 & 1 & 0 & 0 \\ 0 & 0 & \delta_{0,0} & \delta_{0,1} \\ 0 & 0 & \delta_{1,0} & \delta_{1,1} \end{bmatrix} \cdot \begin{bmatrix} 1 & 0 \\ 0 & 1 \\ R_g & 0 \\ 0 & R_g \end{bmatrix} \cdot \begin{bmatrix} i_0(0) \\ i_1(0) \end{bmatrix}. \tag{14}$$

as Fourier transforms, the computation is cumbersome. Finally, the scattering probabilities $\delta_{u,v}$ can also be computed by a numerical simulation based on a simplified light scattering model.[2]

For our purpose, the last method is the most adapted: a high-resolution grid models the printed surface. The value of a grid point corresponds to the local amount of dye (see Fig. 5). The density profile of an isolated ink impact, which was printed on a transparency having the same ink absorbing layer as the paper, was measured under a microscope and approximated by a parabolic function.[23] The resulting ink impact model (see Fig. 5) is used as a stamp. Wherever an ink drop hits the surface of the printed media, the impact model is stamped at the same location on the high resolution grid, where stamp overlapping is additive. This gives an accurate numerical simulation of the behavior of ink printed on high quality paper.

The fraction of area a_u is determined by counting the number of grid points which belong to the same inking level u. The light scattering process can be seen as an exchange of photons between a grid point and its neighbors. In this context, the discrete form of the above mentioned PSF gives the probability for an entering photon to emerge from another grid point. According to Gustavson's studies,[24] this PSF can be approximated by a function $p(r)$ which has a circular symmetry and a strong radial decay:

$$p(r) = \frac{\exp\left[-\frac{r}{d}\right]}{2\pi dr}. \tag{19}$$

Here, d controls the radial extent of the PSF.

The scattering probability $\delta_{u,v}$ equals the weighted sum over the whole grid of points having the inking level u with a neighbor having an inking level v. The weights of the neighbors are given by our discrete PSF.

A Simplified Model of Ink Spreading

In the printing process, inks are partially superposed in order to produce new colors. Under certain circumstances, the overlap of the printed inks causes further spreading of the dyes. This induces a significant dot gain and color deviation as shown in **Color Plate 14 (p. 385)**. Note that the total amount of dyes remains constant throughout the spreading process, and only the spatial distribution is changed. The complex interaction between the inks and the printed surface is strongly related to physical properties like wettability and solvent absorption. As a consequence the inks behave differently on every surface. According to our experience, the local amount of solvent and the state of the surface ("wet" or "dry") are the main parameters to take into account. Printer and paper manufacturers try to minimize the unwanted ink spreading by developing special paper coatings.[25] Nevertheless, ink spreading still induces significant color deviations which must be taken into account.

The ink-spreading phenomenon can be modeled by modifying the size of the impact according to the configuration of its neighboring drop impacts and the state of the surface. Since the amount of dyes remains constant, the maximal density D at the center of the impact must decrease when the area a of the impact increases:

$$D = D_0 \cdot \left(\frac{a_0}{a}\right), \tag{20}$$

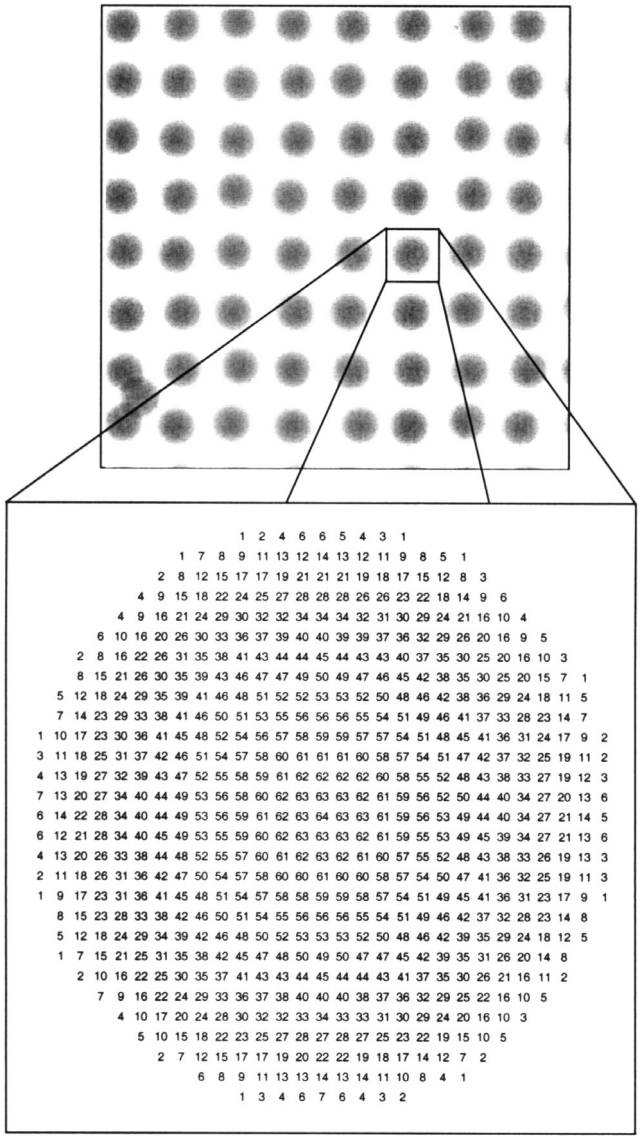

Figure 5. High-resolution grid modeling the printed surface. The value of a grid point corresponds to the local amount of dye. Note that the density profile of an isolated ink impact is parabolic.

where a_0 and D_0 are respectively the area and the maximal density at the center of an isolated impact.

By experimenting on a particular sample, we found a set of empirical rules that are slightly different for each ink-paper combination. First, we analyzed the spreading of a drop printed on a dry surface by estimating under the microscope the enlargement of the impact when it is in contact with an increasing number of neighboring impacts. Second, we estimated the enlargement caused by an ink drop printed on a "wet" surface, i.e., where another drop was already printed, as a function of the number of neighboring impacts. We observed that the higher the number of neighbors covered with ink, the stronger the spreading. A neighboring impact composed of the superposition of two ink drops increases the local amount of solvent. This also influences ink spreading but to a lower extent. These results are summarized in Table I as a set of ink spreading rules that give the enlargement according to the configuration of the ink drop im-

Table I. Empirical impact enlargement rules according to the state of the surface and the configuration of the dot neighbors. The enlargement is given in terms of area percentage. The '*' indicates that the rule in question does not apply.

Surface	Number of neighbors	Number of two-drop neighbors	HP	EPSON
Dry	>1	any	10%	10%
Wet	0	0	0%	32%
Wet	1	0	10%	32%
Wet	1	1	32%	32%
Wet	2	0	32%	32%
Wet	[3…5]	>1	56%	*
Wet	[3…4]	>0	*	44%
Wet	5	>1	*	96%
Wet	6	0	96%	44%
Wet	6	2	140%	140%
Wet	6	[3…5]	189%	189%
Wet	6	6	82%	82%

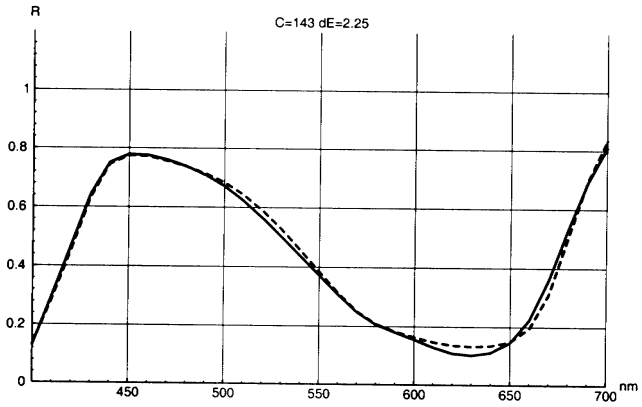

Figure 6. Measured spectrum (continuous line) and predicted spectrum (dashed line) of a halftone cyan sample at level 143 printed with an HP DJ560C. The prediction error is $\Delta E = 2.25$ in CIELAB. (Note that level 0 means 100% ink coverage and level 255 means 0% ink coverage).

pacts. Note that it is better to estimate the ink spreading on a transparency with the same ink-absorbing layer as the paper (if such a transparency is available).

As shown in the previous section, high-resolution grids (one for each ink) are used to simulate the behavior of the inks printed on the substrate. Each simulated impact is stamped on a high-resolution grid and its size is computed according to our empirical ink spreading rules.

Prediction Results

In a first step this model was applied to monochromatic patches. We predicted the spectra of 25 cyan halftone samples generated with Bayer's[26] dithering method and printed using an HP DJ560 ink-jet printer. Note that this device prints colored drops according to a hexagonal grid and the shape of the drop impact is circular. All 25 samples were printed on J21 paper from MPA[27] whose ink absorbing layer has a refractive index of $n = 1.5$. The ink spreading rules for this ink-paper combination are given in Table I in the column labeled "HP". The samples were illuminated with a tungsten light source and their spectra were measured using an integrating sphere combined with a radiometer INSTASPEC II from Oriel.[28] The samples were measured 24 h after being

Table II. Average prediction error in CIELAB, root mean square error and maximal deviation of predicted spectra of the series of cyan samples printed with an HP DJ 560C printer.

Series	Average ΔE	$\sqrt{\frac{\sum \Delta E^2}{n}}$	Maximal ΔE
25 cyan samples	1.40	1.51	2.67

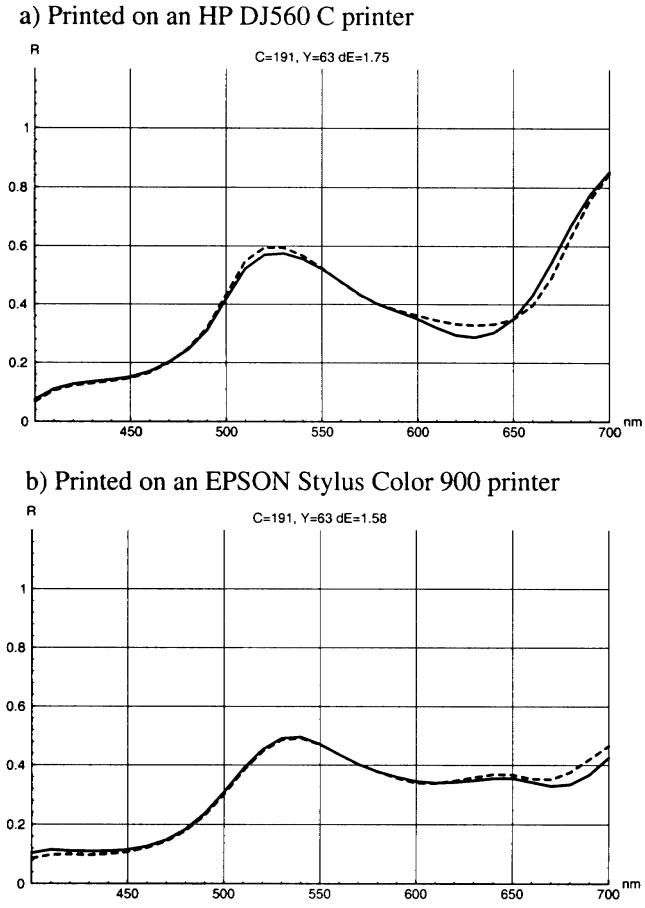

Figure 7. Measured spectra (continuous lines) and predicted spectra (dashed lines) of one halftone green sample (clustered dither) printed on two different printers. The patch is a superposition of a cyan halftone layer (level 191) and a yellow halftone layer (level 127). Note that level 0 means 100% ink coverage and level 255 means 0% ink coverage.

printed. The same instrument was used to measure the reflectance of the paper in order to derive R_g. The absorption spectra of the cyan ink was measured on transparency with the same ink absorbing layer using the same radiometer with collimated light.

Most high quality papers contain fluorescent whitening agents that absorb UV light and emit light in the blue region of the spectrum.[29,32] This light emission is strongly reduced when the paper is covered with ink, since our inks absorb the UV light. Therefore, we separate the reflectance of the paper into two components: R_g and the fluorescent emission. This separation is done with a UV filter. In our approximation, the fluorescent contribution, which depends on the light source, is added to R_g only if no ink is present.

TABLE III. Bayer dither, printed with the HP printer. Measured color, predicted color and color difference in CIELAB

Levels	C=255			C=191			C=127			C=63			C=0		
	a	b	L	a	b	L	a	b	L	a	b	L	a	b	L
Y=255	1.	–3.	91.	–22.	–32.	72.	–41.	–50.	58.	–47.	–60.	50.	–47.	–65.	46.
	1.	–3.	92.	–24.	–30.	72.	–39.	–48.	59.	–45.	–58.	51.	–47.	–66.	45.
	0.3			1.9			2.7			2.3			0.4		
Y=191	1.	27.	90.	–24.	–4.	70.	–46.	–23.	56.	–54.	–30.	49.	–55.	–34.	44.
	1.	25.	91.	–25.	–4.	71.	–45.	–21.	57.	–52.	–28.	50.	–55.	–32.	44.
	1.5			1.6			2.4			2.2			1.9		
Y=127	2.	49.	90.	–29.	14.	67.	–51.	–5.	54.	–57.	–12.	47.	–53.	–16.	44.
	2.	47.	90.	–32.	12.	67.	–48.	–4.	55.	–56.	–12.	48.	–57.	–17.	44.
	1.8			3.7			3.3			1.9			4.7		
Y=63	4.	64.	90.	–35.	25.	65.	–55.	7.	52.	–56.	–1.	47.	–54.	–6.	43.
	3.	62.	90.	–36.	23.	65.	–53.	6.	53.	–56.	–2.	47.	–56.	–8.	43.
	2.3			2.7			2.5			1.5			3.2		
Y=0	5.	75.	89.	–41.	31.	61.	–54.	15.	51.	–57.	7.	45.	–55.	1.	42.
	4.	75.	90.	–43.	30.	62.	–58.	12.	52.	–58.	4.	46.	–55.	2.	42.
	0.9			2.1			5.1			2.9			0.6		

TABLE IV. Clustered dither, printed with the HP printer. Measured color, predicted color and color difference in CIELAB.

Levels	C=255			C=191			C=127			C=63			C=0		
	a	b	L	a	b	L	a	b	L	a	b	L	a	b	L
Y=255	1.	–3.	91.	–15.	–24.	76.	–26.	–39.	65.	–38.	–54.	54.	–47.	–65.	46.
	1.	–3.	92.	–15.	–24.	76.	–26.	–40.	65.	–41.	–55.	53.	–47.	–66.	45.
	0.2			0.9			0.8			3.			1.3		
Y=191	1.	19.	91.	–16.	–5.	75.	–28.	–20.	64.	–42.	–34.	53.	–53.	–43.	44.
	1.	20.	91.	–17.	–4.	75.	–29.	–18.	64.	–44.	–33.	52.	–53.	–42.	44.
	1.2			2.3			2.8			2.2			1.7		
Y=127	2.	38.	90.	–17.	12.	74.	–29.	–4.	63.	–46.	–19.	51.	–56.	–26.	43.
	2.	40.	90.	–20.	12.	73.	–32.	–3.	62.	–46.	–17.	51.	–55.	–24.	44.
	1.4			2.4			2.8			1.1			1.7		
Y=63	4.	59.	89.	–20.	30.	71.	–33.	14.	60.	–49.	–1.	50.	–56.	–9.	43.
	3.	59.	90.	–19.	31.	72.	–33.	13.	60.	–49.	–2.	49.	–56.	–9.	43.
	0.9			1.8			1.2			1.			0.4		
Y=0	5.	75.	89.	–24.	43.	69.	–40.	24.	56.	–54.	9.	47.	–54.	1.	42.
	4.	75.	90.	–22.	43.	70.	–39.	23.	58.	–55.	8.	47.	–55.	2.	42.
	0.9			2.6			2.1			1.7			1.		

TABLE V. Bayer dither, printed with the EPSON printer. Measured color, predicted color and color difference in CIELAB.

Levels	C=255			C=191			C=127			C=63			C=0		
	a	b	L	a	b	L	a	b	L	a	b	L	a	b	L
Y=255	1.	–2.	94.	–19.	–33.	72.	–33.	–54.	57.	–37.	–65.	48.	–41.	–73.	41.
	1.	–2.	94.	–18.	–32.	73.	–35.	–54.	57.	–39.	–63.	50.	–43.	–70.	43.
	0.1			2.1			2.			3.2			3.8		
Y=191	3.	35.	92.	–23.	5.	68.	–37.	–15.	54.	–44.	–24.	45.	–49.	–32.	38.
	3.	35.	92.	–22.	2.	68.	–38.	–18.	53.	–43.	–27.	47.	–48.	–35.	40.
	0.8			3.1			3.3			3.2			4.		
Y=127	5.	62.	91.	–20.	28.	67.	–39.	6.	51.	–44.	–3.	43.	–47.	–10.	37.
	7.	64.	90.	–19.	27.	66.	–39.	5.	50.	–45.	–4.	44.	–48.	–10.	39.
	2.6			1.5			1.7			1.9			2.4		
Y=63	8.	76.	90.	–19.	39.	65.	–38.	17.	50.	–43.	6.	42.	–45.	–1.	37.
	9.	76.	90.	–18.	37.	64.	–39.	15.	50.	–44.	6.	42.	–45.	1.	36.
	1.			2.2			2.6			0.5			2.2		
Y=0	10.	87.	89.	–17.	48.	64.	–38.	23.	48.	–42.	11.	40.	–42.	5.	36.
	11.	88.	89.	–16.	48.	63.	–38.	23.	48.	–42.	12.	39.	–45.	7.	36.
	1.3			1.2			0.8			1.7			3.2		

TABLE VI. Clustered dither, printed with the EPSON printer. Measured color, predicted color and color difference in CIELAB.

Levels	C=255			C=191			C=127			C=63			C=0		
	a	b	L	a	b	L	a	b	L	a	b	L	a	b	L
Y=255	1.	−2.	94.	−12.	−26.	76.	−19.	−42.	64.	−30.	−58.	52.	−42.	−73.	41.
	1.	−2.	94.	−12.	−25.	77.	−21.	−41.	65.	−33.	−58.	53.	−43.	−70.	43.
	0.2			2.3			2.4			3.4			3.9		
Y=191	3.	26.	92.	−14.	−0.	73.	−20.	−14.	62.	−31.	−30.	50.	−45.	−44.	39.
	3.	26.	92.	−14.	1.	74.	−22.	−13.	63.	−35.	−29.	50.	−46.	−43.	41.
	0.3			1.6			2.3			4.1			2.7		
Y=127	6.	46.	91.	−14.	16.	71.	−21.	2.	59.	−30.	−12.	49.	−45.	−26.	38.
	6.	48.	91.	−13.	17.	71.	−23.	3.	60.	−34.	−10.	49.	−47.	−22.	39.
	1.4			1.7			2.2			4.5			4.9		
Y=63	8.	68.	90.	−12.	36.	69.	−22.	18.	57.	−32.	4.	47.	−44.	−7.	37.
	9.	70.	90.	−11.	38.	69.	−24.	19.	57.	−35.	5.	46.	−46.	−5.	37.
	1.4			1.6			1.6			4.			3.6		
Y=0	10.	87.	89.	−10.	54.	67.	−21.	35.	55.	−34.	17.	44.	−43.	4.	36.
	11.	88.	89.	−7.	57.	69.	−22.	34.	54.	−36.	17.	43.	−45.	7.	36.
	1.5			4.6			1.8			2.7			3.2		

TABLE VII. Average prediction error in CIELAB, root mean square error and maximal deviation for each cyan–yellow series of predicted spectra.

Series	Average ΔE	$\sqrt{\frac{\sum \Delta E^2}{n}}$	Maximal ΔE
Bayer dither on HP printer	2.25	2.53	5.08
Clustered dither on HP printer	1.57	1.75	2.95
Bayer dither on EPSON printer	2.10	2.34	3.96
Clustered dither on EPSON printer	2.56	2.85	4.92

TABLE VIII. Average prediction error in ΔE94, root mean square error and maximal deviation for each cyan–yellow series of predicted spectra.

Series	Average ΔE	$\sqrt{\frac{\sum \Delta E^2}{n}}$	Maximal ΔE
Bayer dither on HP printer	1.16	1.26	2.30
Clustered dither on HP printer	0.94	1.06	1.84
Bayer dither on EPSON printer	1.32	1.52	3.08
Clustered dither on EPSON printer	1.48	1.67	2.99

For good prediction accuracy, five inking levels are taken into account. This implies the use of larger matrices in Eq. 14. Furthermore, the grid point corresponds to a square surface element of 5×5 μm. In accordance with Oittinen's study,[30] the extent of our discrete PSF has a radius of about 100μm. As a consequence, the value of d in Eq. 19 is about 20 μm. Note that at 300 dpi, the distance between two dot centers is 85 μm. The integration of the PSF over the area of a neighboring grid point gives the weight of this point.

Using our model and mathematical framework, we computed the spectra of the 25 halftoned cyan samples with an average prediction error of $\Delta E = 1.4$ and a maximal error of $\Delta E = 2.7$ in CIELAB. An example of a predicted spectrum is given in Fig. 6, and the results are summarized in Table II.

In a second step the model predicted the spectra of samples printed with two inks, cyan and yellow. We produced four series of 25 samples i.e., a total of 100 samples. They correspond to the four combinations obtained by using two different halftoning methods with two different printers (having different inks and papers). The halftone methods used were a clustered dither algorithm with 33 levels of gray and Bayer's[26] dithering method. Two series were printed with an HP DJ560 ink-jet printer on J21 paper from MPA.[27] Two other series were printed with an EPSON Stylus Color 900 ink-jet printer on "EPSON glossy photo quality" paper.[31] All samples were measured with the same equipment used in the monochrome case. The EPSON Stylus Color 900 printer was used in its 360-dpi mode. It also uses a hexagonal grid for colored inks, but its drop impact is elliptic.

We simulated these samples on the high-resolution grids using the previously described ink spreading model and light scattering model. As in the case of the monochromatic samples, the computer counted the grid points and their neighbors in order to find the relative area a_u occupied by each ink combination u and the scattering coefficients $\delta_{u,v}$ (see in the section **Simplified Light Scattering Model**). Because we consider five inking levels per ink, a total of twenty-five combinations must be taken into account. The computation of the reflection spectrum is the same as in the monochromatic case except that larger matrices are used in Eq. 14.

The average prediction error between measured and predicted spectra is about $\Delta E = 2.1$ and the maximal error is $\Delta E = 5$ in CIELAB. Two examples are given in Fig. 7, and the results are listed in Tables III, IV, V and VI. A summary is given in Table VII; the $\Delta E94$ values were also computed and they are given in Table VIII. Note that when ink spreading is not taken into account, the average prediction error is about $\Delta E = 10$ in CIELAB.

Conclusions

We introduced a new mathematical framework based on matrices. This global approach incorporates all significant physical-contributing phenomena. We introduced light scattering coefficients that could also be changed to suit other models of light scattering in paper. We have shown that classical results such as the Murray–Davis, the Williams–Clapper and the Clapper–Yule formulas correspond to particular cases of our model.

We modeled the spreading process by enlarging the drop impact according to the configuration of its neighbors and the state of the surface. The printed surface was simulated using high-resolution grids. This allowed us to compute the relative areas occupied by the various ink-combinations and the corresponding light scattering coefficients $\delta_{u,v}$.

The spectra of halftone samples produced with one ink were predicted with an average prediction error of about $\Delta E = 1.4$ in CIELAB. For two halftone ink layers, we also achieved good spectral predictions with an average error of about $\Delta E = 2.1$ in CIELAB.

Currently we are extending the experimental set to other ink combinations and other ink-jet printers. The complexity of ink spreading requires deeper investigation in order to predict the behavior of three ink combinations.

Acknowledgments. We would like to thank Dr. P. Heinzer from MPA for providing useful information on ink-jet paper, and the Swiss National Science Foundation (grant No. 21-54127.98) for supporting the project.

References

1. J. S. Arney, T. Wu and C. Blehm, Modeling the Yule–Nielsen Effect on Color Halftones, *J. Imaging Sci. Technol.* **42,** 335–340 (1998).
2. S. Gustavson, *Dot Gain in Color Halftones*, PhD thesis No. 492, Linköping University, Linköping, Sweden, September 1997.
3. G. L. Rogers, Effect of Light Scatter on Halftone Color, *J. Opt. Soc. Am. A* **15,** 1813–1821 (1998).
4. P. Kubelka and F. Munk, Ein Beitrag zur Optik der Farbanstriche, *Z. tech. Physik* **12,** 593–601 (1931).
5. W. E. Boyce and R. C. DiPrima, *Elementary Differential Equations and Boundary Value Problems*, 6th ed., John Wiley & Sons, New York, 1997, pp. 401–405.
6. J. H. Nobbs, *Colour Physics for Industry*, R. McDonald Ed., 2nd ed., The Society of Dyers and Colourists, Bradford, UK, 1997, p. 306.
7. P. Emmel, *Modèles de Prédiction Couleur Appliqués à l'Impression Jet d'Encre*, PhD thesis No. 1857, Ecole Polytechnique Fédérale de Lausanne (EPFL), Lausanne, Switzerland, 1998, pp. 55–58, http://diwww.epfl.ch/w3lsp/publications/colour/thesis-emmel.html (in French).
8. P. Emmel and R. D. Hersch, Towards a Color Prediction Model for Printed Patches, *IEEE Computer Graphics and Applications*, **19,** 54–60 (1999).
9. D. B. Judd and G. Wyszecki, *Color in Business, Science and Industry*, 3rd ed., John Wiley & Sons, 1975, pp. 426–431.
10. See reference 6, p. 299.
11. See reference 9, pp. 415–417.
12. See reference 6, pp. 304–307.
13. D. B. Judd, Fresnel Reflection of Diffusely Incident Light, *J. Nat'l. Bureau of Standards*, **29,** 329–332 (1942).
14. J. L. Saunderson, Calculation of the Color Pigmented Plastics, *J. Opt. Soc. Am.* **32,** 727–736 (1942).
15. See reference 7, pp. 77–78.
16. F. C. Williams and F. R. Clapper, Multiple Internal Reflections in Photographic Color Prints, *J. Opt. Soc. Am.* **43,** 595–599 (1953).
17. J. S. Arney, Probability Description of the Yule–Nielsen Effect: I, *J. Imaging Sci. Technol.* **41,** 633–636 (1997).
18. H. E. J. Neugebauer, Die theoretischen Grundlagen des Mehrfarbenbuchdrucks, *Z. wiss. Photogr.* **36**(4), 73–89 (1937).
19. F. R. Clapper and J. A. C. Yule, The Effect of Multiple Internal Reflections on the Densities of Halftone Prints on Paper, *J. Opt. Soc. Am.* **43,** 600–603 (1953).
20. H. R. Kang, *Color Technology for Electronic Imaging Devices*, SPIE Optical Engineering Press, Bellingham WA, 1997, pp. 42–43.
21. F. R. Ruckdeschel and O. G. Hauser, Yule–Nielsen effect in printing: a physical analysis, *Appl. Opt.* **17,** 3376–3383 (1978).
22. G. L. Rogers, Optical dot gain in halftone print, *J. Imaging Sci. Technol.* **41,** 643–656 (1997).
23. See reference 7, p. 114.
24. See reference 2, p. 55.
25. A. Owatari et al., Ink Jet Recording Medium, US Pat. 5,928,787 (1999).
26. B. E. Bayer, An Optimum Method for Two-Level Rendition of Continuous-Tone Pictures, *IEEE 1973 International Conference on Communications*, Vol. 1, IEEE, 1973, pp. 26-11—26-15.
27. http://www.mpa.ch
28. http://www.LOT-Oriel.com
29. See reference 6, p. 339.
30. P. Oittinen and H. Saarelma, Influence of optical surface properties of paper on information capacity, *Paperi ja puu – Paper and Timber* **75,** 66–71 (1993).
31. http://www.epson.com
32. G. Wyszecki and W. S. Stiles, *Color Science: Concepts and Methods, Quantitative Data and Formulae*, 2nd ed., John Wiley & Sons, 1982, pp. 235–240.

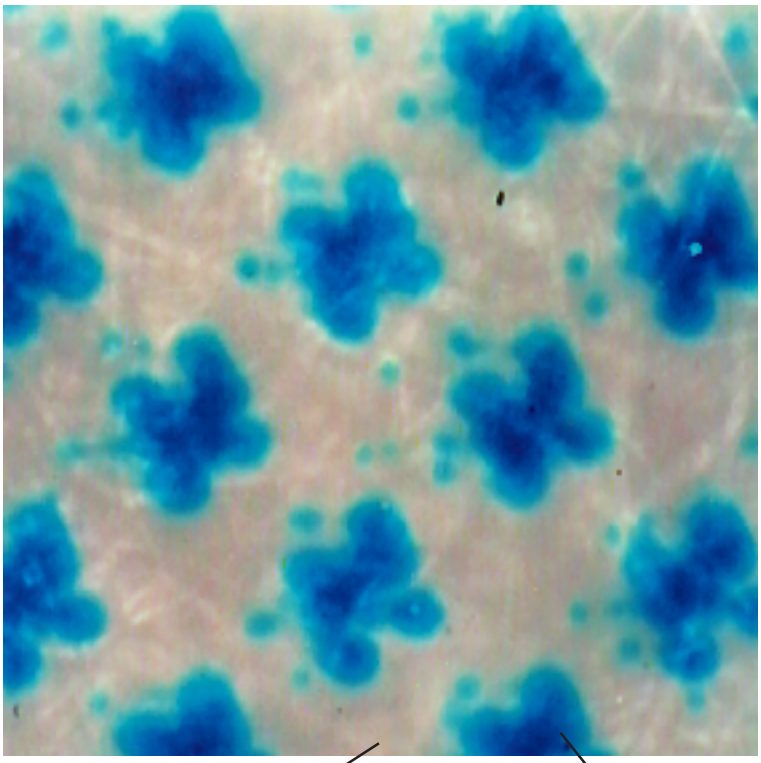

(a)

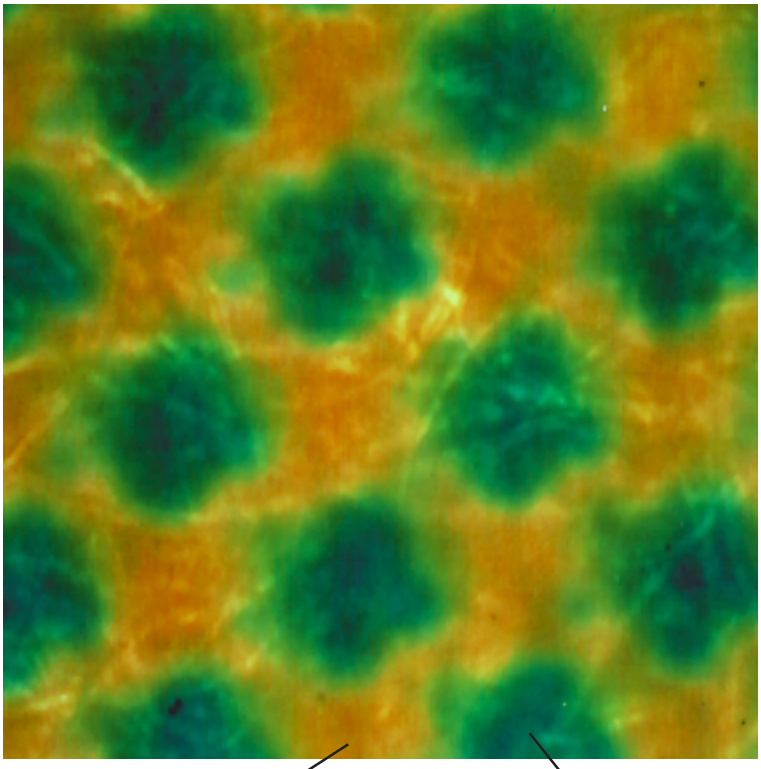

(b)

Plate 21. Microscopic views of a halftoned cyan sample (a) and of a green halftoned sample (b). The green sample (b) is made of the same cyan layer as (a) and covered with a uniform yellow layer . Note the enlargement of the cyan clusters in (b) [Emmel and Hersch, pp. 345–353].